



Research article

Neural networks-based adaptive fault-tolerant control for a class of nonstrict-feedback nonlinear systems with actuator faults and input delay

Mohamed Kharrat¹ and Hadil Alhazmi^{2,*}

¹ Department of Mathematics, College of Science, Jouf University, P.O. Box 2014, Sakaka, Saudi Arabia

² Department of Mathematical Sciences, College of Science, Princess Nourah Bint Abdulrahman University, P.O. Box 84428, Riyadh 11671, Saudi Arabia

* **Correspondence:** Email: hnalhazmi@pnu.edu.sa.

Abstract: This paper addresses the challenge of adaptive control for nonstrict-feedback nonlinear systems that involve input delay, actuator faults, and external disturbance. To deal with the complexities arising from input delay and unknown functions, we have incorporated Pade approximation and radial basis function neural networks, respectively. An adaptive controller has been developed by utilizing the Lyapunov stability theorem and the backstepping approach. The suggested method guarantees that the tracking error converges to a compact neighborhood that contains the origin and that every signal in the closed-loop system is semi-globally uniformly ultimately bounded. To demonstrate the efficacy of the proposed method, an electromechanical system application example, and a numerical example are provided. Additionally, comparative analysis was conducted between the Pade approximation proposed in this paper and the auxiliary systems in the existing method. Furthermore, error assessment criteria have been employed to substantiate the effectiveness of the proposed method by comparing it with existing results.

Keywords: backstepping method; actuator faults; nonlinear systems; input delay; electromechanical system

Mathematics Subject Classification: 92B20, 93C10, 93C40

1. Introduction

In recent decades, there has been considerable focus on the control challenges associated with nonlinear systems, driven by the widespread occurrence of nonlinear behavior in modern control systems [1]. Various control strategies, including adaptive output feedback control, adaptive event-triggered control, adaptive backstepping control, and adaptive sliding mode control have been

developed [2, 3]. The backstepping control technique offers a systematic approach to tackling tracking control problems in nonlinear systems without the need to satisfy matching conditions. This technique involves breaking down the intricate nonlinear system into multiple subsystems and subsequently designing a virtual controller for each subsystem until the actual control law is derived [4]. In previous works, adaptive backstepping controllers and variable structure adaptive backstepping controllers were introduced to address the control problems of specific systems. However, for certain nonlinear systems, obtaining accurate dynamic models proves exceedingly challenging. To address this challenge, researchers have introduced neural networks (NNs) and fuzzy logic systems (FLSs) [5]. Given their ability to identify unknown nonlinear functions, the application of NNs and FLSs in the control of nonlinear systems has garnered significant interest and various studies in this domain have been conducted [6–8]. For example, an adaptive NN-based decentralized control approach has been formulated for interconnected nonlinear systems [9]. Additionally, an adaptive method has been reported for stochastic nonlinear systems by using fuzzy approximation and output feedback control [10]. However, it is important to clarify that the studies mentioned above did not consider the fault-tolerance aspect of the controlled system.

Actuators and sensors regularly experience operational disruptions and faults in real-world manufacturing environments, such as those involving flight control systems, satellite operations, and nuclear power facilities [11]. These faults can result in unsatisfactory system performance and, in severe cases, lead to instability. Ensuring system reliability and stability under all circumstances is crucial. As a result, it is crucial to devise an effective fault-tolerant control scheme that ensures the maintenance of stable and satisfactory control performance, even when faults are present [12]. Actuators ultimately age or breakdown entirely due to the increasing complexity and automation of modern control systems, particularly when they are subjected to demanding and prolonged continuous operations [13]. Actuator failures are common in many real-world applications, such as offshore ship-mounted cranes, two-stage chemical reactors and highly adaptable airplanes [14]. To minimize the negative impacts of faults on the system and get it as close to its pre-fault state as possible, fault-tolerant control is required. Adaptive control can simultaneously achieve optimal performance by dynamically modifying the controller design. As a result, combining fault-tolerant control with adaptive control has become a primary area of research to improve the security and dependability of industrial systems [15]. For instance, using the command filter technique, an adaptive fault-tolerant control issue for switched nonlinear systems has been reported [16]. Furthermore, an adaptive fault-tolerant control problem has been explored for a class of nonlinear large-scale systems under the impact of dead-zone nonlinearity [17]. In addition, under the influence of uncertainties in mismatched parameters and disturbances, an adaptive fault-tolerant control problem has been explored for nonaffine nonlinear systems [18]. A model-free adaptive fault-tolerant control technique, relying on NNs, has been documented for discrete-time nonlinear systems in the presence of sensor faults [19]. Despite these accomplishments, to the best of our knowledge, there has been no attention given to fault-tolerant control considering input delay in the existing literature.

Moreover, input delays can stem from the inherent characteristics of the plant or external factors within the system, such as computation time or sensor measurements [20]. This occurrence has the potential to result in a decline in system performance, or even induce instability [21]. Recent efforts have introduced various approaches to tackle adaptive control schemes for nonlinear systems grappling with input delays [22, 23]. In [24], the authors have presented a NN-based adaptive control

strategy for nonlinear systems facing state constraints and input delays. For single-input single-output uncertain systems with unmodeled dynamics and encompassing unknown constant time delays, an adaptive controller has been formulated using a backstepping design [25]. To address the adaptive fuzzy tracking control problem for nonlinear systems with input delays and output constraints, Pade approximation has been employed [26]. Furthermore, the exploration of adaptive output tracking control for disturbed multiple-input multiple-output switched uncertain nonlinear systems with input delays has been reported [27]. The authors of [28] proposed an adaptive fuzzy control methodology specifically for high-order nonlinear time-delay systems characterized by input saturation and state constraints.

Inspired by these considerations, here, we have undertaken the challenge of formulating an adaptive controller for nonstrict-feedback nonlinear systems featuring actuator faults, external disturbances, and input delays. Notably, considering the existing literature, the following contributions distinguish this work:

- (1) Compared with the existing results [1, 15], this paper addresses the problem of nonlinear systems with a nonstrict-feedback structure. The proposed control scheme deals with both input delay and actuator faults in nonlinear systems. Instead of employing the auxiliary system from previous research [29], this study utilizes the Pade approximation method to address the issue of input delay. It introduces the variable x_{n+1} to handle input delay, thereby simplifying the design process. In addition, external disturbance is also considered in this work. This demonstrates the versatility and real-world usefulness of the proposed control strategy.
- (2) By utilizing the capabilities of radial basis function NNs, this study employs a backstepping method to create an adaptive fault-tolerant controller through the application of Lyapunov stability theory. The controller ensures that all signals in the closed-loop systems are bounded and tracking errors converge to a small area around the starting point. The effectiveness of the proposed method is confirmed through comparisons with existing results by using error assessment criteria.

This article is organized into the following sections. The problem formulation and preliminary information are provided in Section 2. Section 3 presents the main results. The results of the simulation are then covered in Section 4, and the conclusion is given in Section 5.

2. System statement and preliminaries

Consider the following type of nonstrict-feedback nonlinear system with input delays and actuator faults:

$$\begin{cases} \dot{x}_i = f_i(x) + x_{i+1} + d_i(t), & 1 \leq i \leq n-1, \\ \dot{x}_n = f_n(x) + u(v(t-\tau)) + d_n(t), \\ y = x_1, \end{cases} \quad (2.1)$$

where $x = [x_1, \dots, x_n]^T$ is the state variable, $f_i(\cdot)$ denotes the unknown nonlinear function with $f_i(0) = 0$, v is the controller input to be designed, u is the system input that is subject to actuator fault, τ is the input delay, which is a positive constant, y is the system output, $d_i(\cdot)$ represents the external disturbance, and $d_i(\cdot)$ satisfies $|d_i(\cdot)| \leq \bar{d}_i$, with \bar{d}_i being the constant.

In this study, the input delay problem is addressed by estimating the input delay of the systems using

the Pade approximation, as described in [30]. The Pade approximation is characterized as follows:

$$\mathcal{L}\{u(v(t - \tau))\} = \exp(-\tau s)\mathcal{L}\{u(v(t))\} \approx \frac{1 - \frac{\tau s}{2}}{1 + \frac{\tau s}{2}}\mathcal{L}\{u(v(t))\}, \quad (2.2)$$

where s is the Laplace variable and $\mathcal{L}\{u(v(t))\}$ is the Laplace transform of $u(t)$.

Describe the new variable x_{n+1} as follows:

$$\mathcal{L}\{x_{n+1}(t)\} = \frac{1 - \frac{\tau s}{2}}{1 + \frac{\tau s}{2}}\mathcal{L}\{u(v(t))\} + \mathcal{L}\{u(v(t))\}. \quad (2.3)$$

By the inverse Laplace transform and $\rho = \frac{2}{t_d}$, one has

$$\dot{x}_{n+1} = \frac{4}{\tau}u(v(t)) - \frac{2}{\tau}x_{n+1} = 2\rho u(v(t)) - \rho x_{n+1}. \quad (2.4)$$

By using (2.2)–(2.4), the system (2.1) can be rewritten as follows:

$$\begin{cases} \dot{x}_i = f_i(x_i) + x_{i+1} + d_i(t), & 1 \leq i \leq n-1, \\ \dot{x}_n = f_n(x_n) + x_{n+1} - u(v(t)) + d_n(t), \\ \dot{x}_{n+1} = -\rho x_{n+1} + 2\rho u(v(t)), \\ y = x_1, \end{cases} \quad (2.5)$$

where $u(v(t))$ denotes the system input that is subject to actuator fault described by

$$u(v(t)) = \lambda(t, t_\lambda)v + u_r(t, t_r), \quad (2.6)$$

where $\lambda(t, t_\lambda) \in [0, 1]$ indicates the effectiveness of the actuation. v is a control signal, and t_λ denotes the time instant at which an actuation effectiveness fault will occur. An uncontrollable additive actuation fault is represented by $u_r(t, t_r)$, and the instant an additive actuation fault occurs is indicated by t_r [31].

By using (2.6), the nonlinear system (2.5) can be rewritten as follows:

$$\begin{cases} \dot{x}_i = f_i(x_i) + x_{i+1} + d_i(t), & 1 \leq i \leq n-1, \\ \dot{x}_n = f_n(x_n) + x_{n+1} - \lambda(t, t_\lambda)v - u_r(t, t_r) + d_n(x, t), \\ \dot{x}_{n+1} = -\rho x_{n+1} + 2\rho\lambda(t, t_\lambda)v + 2\rho u_r(t, t_r), \\ y = x_1. \end{cases} \quad (2.7)$$

Remark 2.1. x_{n+1} is a newly introduced variable that manages the input delay. x_{n+1} can be considered an intermediate rather than the system state variable [30].

The control goal is to formulate an adaptive fault-tolerant controller for the system (2.1) ensures that all signals within the closed-loop exhibit semi-globally uniformly ultimately bounded (SGUUB) behavior, and that the tracking error converges to a compact region around the origin. To achieve this goal, the following assumptions and lemmas are necessary.

Assumption 2.1. [1] The desired trajectory signal $y_d(t)$ and its time derivatives up to the n th order are assumed to be continuous and bounded.

Assumption 2.2. [31] The unknown time-varying functions $\lambda(t, t_l)$ and $u_r(t, t_r)$ are bounded. Thus, there exist positive constants λ_{\min} and u_{\max} such that $\lambda_{\min} < \lambda(t, t_l) \leq 1$ and $|u_r(t, t_r)| \leq u_{\max}$.

Remark 2.2. Assumption 2.1 ensures the boundedness of the reference signal $y_d(t)$ and its time derivatives $y_d^{(n)}(t)$, thus guaranteeing the boundedness of all variables throughout the backstepping derivation. This assumption is a standard practice in the design of adaptive controllers, has been demonstrated in various works, including [1, 2, 5, 6]. The control gain $\lambda(t, t_l)$ and the uncontrollable additive actuation fault $u_r(t, t_r)$ are unknown, as stated in Assumption 2.2. As such, the traditional stability requirement is no longer applicable [31].

Radial basis function neural networks (RBFNNs). In this work, an RBFNN [32] is used to approximate the continuous function $f_i(X) : \mathbb{R}^n \rightarrow \mathbb{R}$. The RBFNN is expressed in the following form:

$$f(X) = W^T S(X), \quad (2.8)$$

where $X \in \Omega_X \subset \mathbb{R}^q$ represents the input vector and $W = [w_1, \dots, w_l]^T \in \mathbb{R}^l$ denotes the weight vector of the RBFNN, where $l(> 1)$ is the number of nodes. Additionally, $S(X) = [s_1(X), \dots, s_l(X)]^T \in \mathbb{R}^l$ is the basis function vector, and $s_i(X)$ is given by

$$s_i(X) = \exp\left(-\frac{(X - \mu_i)^T(X - \mu_i)}{\zeta^2}\right), \quad 1 \leq i \leq l, \quad (2.9)$$

where $\mu_i = [\mu_{i1}, \dots, \mu_{iq}]^T$ and ζ denotes the center and the width of the Gaussian function.

As illustrated in [32], the function $f(X)$ is continuous and defined on a compact set Ω_X . For any $\varepsilon > 0$, there exists an RBFNN represented as $W^{*T} S(X)$ such that the following relationship holds:

$$f(X) = W^{*T} S(X) + \delta(X), \quad \forall X \in \Omega_X, \quad (2.10)$$

where $\delta(X)$ represents the approximation error with $|\delta(X)| < \varepsilon$ i, W^* is the ideal weight vector defined as

$$W^* = \arg \min_{W \in \mathbb{R}^l} \sup_{X \in \Omega_X} |f(X) - W^T S(X)|. \quad (2.11)$$

Lemma 2.1. [32] Let $S(X) = [s_1(X), \dots, s_l(X)]^T$ denote the basis function vector of the RBFNN, and $X = [x_1, \dots, x_n]^T$ represent the input vector. For an arbitrary integer $m \leq n$, let $X_m = [x_1, \dots, x_m]^T$. The following inequality holds:

$$\|S(X)\|^2 \leq \|S(X_m)\|^2. \quad (2.12)$$

Lemma 2.2. [4] For all $(m, n) \in \mathbb{R}^2$ and $\varepsilon > 0$, the following inequality holds:

$$mn \leq \frac{\varepsilon^p}{p} |m|^p + \frac{1}{q\varepsilon^p} |n|^q, \quad (2.13)$$

where $p > 1$, $q > 1$, and $(p - 1)(q - 1) = 1$.

Remark 2.3. Lemma 2.1 explains an important and basic structural feature of RBFNNs. It is important to emphasize that, in the context of backstepping design, Lemma 2.1 plays a crucial role in managing the complete state variables [32].

3. Adaptive fault-tolerant controller design and stability analysis

In this section, a design procedure for an adaptive fault-tolerant controller based on the backstepping method for the system (2.1) will be developed. The proposed design procedure consists of n steps, designed for an n -th order system. To design the controller, the first step involves a change of coordinates given by

$$\begin{cases} e_1 = x_1 - y_d, \\ e_i = x_i - \alpha_{i-1}, \quad i = 1, 2, \dots, n-1, \\ e_n = x_n - \alpha_{n-1} + \frac{x_{n+1}}{\rho}, \end{cases} \quad (3.1)$$

where α_{i-1} stands for the virtual control law that will be introduced later. To obtain the main results, the controller design process is separated into n steps.

Step 1. By using (2.7) and (3.1), the time derivative of e_1 is given by

$$\dot{e}_1 = \dot{x}_1 - \dot{y}_d = f_1(x) + x_2 + d_1(t) - \dot{y}_d. \quad (3.2)$$

Choose the following Lyapunov function V_1 as follows:

$$V_1 = \frac{1}{2}e_1^2 + \frac{1}{2r_1}\tilde{\theta}_1^2, \quad (3.3)$$

where $e_1 = x_1 - y_d$, $r_1 > 0$ is a design constant, and $\tilde{\theta}_1 = \theta_1 - \hat{\theta}_1$ represents the estimation error, with $\hat{\theta}_1$ denoting the estimate of the unknown parameter θ_1 , defined as $\theta_1 = \|W_1^*\|^2$.

Then, by taking the time derivative of V_1 , one has

$$\begin{aligned} \dot{V}_1 &= e_1\dot{e}_1 - \frac{1}{r_1}\tilde{\theta}_1\dot{\hat{\theta}}_1 \\ &= e_1(f_1(x) + e_2 + \alpha_1 + d_1(t) - \dot{y}_d) - \frac{1}{r_1}\tilde{\theta}_1\dot{\hat{\theta}}_1 \\ &= e_1(\bar{f}_1(X_1) + e_2 + \alpha_1 + d_1(t)) - \frac{1}{2}e_1^2 - \frac{1}{r_1}\tilde{\theta}_1\dot{\hat{\theta}}_1, \end{aligned} \quad (3.4)$$

where $\bar{f}_1(X_1) = f_1(x) + \frac{1}{2}e_1 - \dot{y}_d$.

In (3.4), it is evident that $\bar{f}_1(X_1)$ contains the unknown smooth function f_1 . Consequently, the RBFNN $W_1^{*T}S(X_1)$ is employed to characterize $\bar{f}_1(X_1)$ in such a way that, for any given constant $\varepsilon_1 > 0$,

$$\bar{f}_1(X_1) = W_1^{*T}S_1(X_1) + \delta_1(X_1), \quad |\delta_1(X_1)| \leq \varepsilon_1, \quad (3.5)$$

where $X_1 = [x_1, \dots, x_n]^T$, and $\delta_1(Z_1)$ represents the estimation error.

By utilizing Lemmas 2.1 and 2.2, one has

$$\begin{aligned} e_1\bar{f}_1(X_1) &= e_1(W_1^{*T}S_1(X_1) + \delta_1(X_1)) \\ &\leq |e_1|(\|W_1^*\|\|S_1(X_1)\| + \varepsilon_1) \\ &\leq |e_1|(\|W_1^*\|\|S_1(Z_1)\| + \varepsilon_1) \\ &\leq \frac{1}{2a_1^2}e_1^2\theta_1S_1^T(Z_1)S_1(Z_1) + \frac{a_1^2}{2} + \frac{e_1^2}{2} + \frac{\varepsilon_1^2}{2}, \end{aligned} \quad (3.6)$$

where $\theta_1 = \|W_1^*\|^2$, $Z_1 = [x_1]^T$, and $a_1 > 0$ is a constant.

By using Young's inequality, one has

$$e_1 d_1(t) \leq \frac{e_1^2}{2} + \frac{\bar{d}_1^2}{2}, \quad (3.7)$$

where $\bar{d}_1 > 0$ is a constant.

The design of the virtual control law α_1 is formulated as follows:

$$\alpha_1 = -k_1 e_1 - \frac{1}{2a_1^2} e_1 \hat{\theta}_1 S_1^T(Z_1) S_1(Z_1), \quad (3.8)$$

where $k_1 > 0$ and $a_1 > 0$ are the design parameters.

By using Lemma 2.2 and (3.8), one has

$$e_1 \alpha_1 \leq -k_1 e_1^2 - \frac{1}{2a_1^2} e_1^2 \hat{\theta}_1 S_1^T(Z_1) S_1(Z_1). \quad (3.9)$$

By incorporating (3.6)–(3.9) into (3.4), we have

$$\dot{V}_1 \leq -k_1 e_1^2 + \left(\frac{1}{2a_1^2} e_1^2 S_1^T(Z_1) S_1(Z_1) \right) (\theta_1 - \hat{\theta}_1) + \frac{\bar{d}_1^2}{2} + \frac{a_1^2}{2} + \frac{e_1^2}{2} + \frac{\varepsilon_1^2}{2} - \frac{1}{r_1} \tilde{\theta}_1 \dot{\hat{\theta}}_1. \quad (3.10)$$

Given that $\tilde{\theta}_1 = \theta_1 - \hat{\theta}_1$, (3.10) becomes

$$\dot{V}_1 \leq -k_1 e_1^2 + \frac{\bar{d}_1^2}{2} + \frac{a_1^2}{2} + \frac{e_1^2}{2} + \frac{\varepsilon_1^2}{2} + \frac{1}{r_1} \tilde{\theta}_1 \left(\frac{1}{2a_1^2} r_1 e_1^2 S_1^T(Z_1) S_1(Z_1) - \dot{\hat{\theta}}_1 \right). \quad (3.11)$$

The adaptive law $\dot{\hat{\theta}}_1$ is formulated as follows:

$$\dot{\hat{\theta}}_1 = \frac{r_1}{2a_1^2} e_1^2 S_1^T(Z_1) S_1(Z_1) - \vartheta_1 \hat{\theta}_1, \quad \hat{\theta}_1(0) \geq 0, \quad (3.12)$$

where $r_1 > 0$ and $a_1 > 0$ represent the design parameters.

By substituting (3.12) into (3.11), one has

$$\dot{V}_1 \leq -k_1 e_1^2 + e_1 e_2 + \frac{1}{r_1} \vartheta_1 \tilde{\theta}_1 \hat{\theta}_1 + \frac{a_1}{2} + \frac{\varepsilon_1^2}{2} + \frac{\bar{d}_1^2}{2}. \quad (3.13)$$

Step i ($i = 1, 2, \dots, n-1$). According to (3.1) and (2.7), the time derivative of e_i is given by

$$\dot{e}_i = \dot{x}_i - \dot{\alpha}_{i-1} = f_i(x) + x_{i+1} + d_i(t) - \dot{\alpha}_{i-1}. \quad (3.14)$$

We can obtain the derivative of α_{i-1} as follows:

$$\dot{\alpha}_{i-1} = \sum_{j=0}^{i-1} \frac{\partial \alpha_{i-1}}{\partial y_d^{(j)}} y_r^{(j+1)} + \sum_{j=1}^{i-1} \frac{\partial \alpha_{i-1}}{\partial x_j} (f_j(x) + x_{j+1} + d_j(x, t)) + \sum_{j=1}^{i-1} \frac{\partial \alpha_{i-1}}{\partial \theta_j} \dot{\theta}_j. \quad (3.15)$$

Consider a Lyapunov function as follows:

$$V_i = V_{i-1} + \frac{1}{2}e_i^2 + \frac{1}{2r_i}\tilde{\theta}_i^2, \quad (3.16)$$

where $e_i = x_i - \alpha_{i-1}$, $\tilde{\theta}_i = \theta_i - \hat{\theta}_i$ is the estimation error, and $r_i > 0$ is a design constant.

Further, the dynamics of V_i are given by

$$\dot{V}_i \leq \dot{V}_{i-1} + e_i(f_i(x) + e_{i+1} + \alpha_i + d_i(t) - \dot{\alpha}_{i-1}) - \frac{1}{r_i}\tilde{\theta}_i\dot{\hat{\theta}}_i. \quad (3.17)$$

The derivative of V_{i-1} is given as follows:

$$\dot{V}_{i-1} \leq -\sum_{j=1}^{i-1} k_j e_j^2 + e_{i-1}e_i + \sum_{j=1}^{i-1} \frac{1}{r_j} \vartheta_j \tilde{\theta}_j \hat{\theta}_j + \sum_{j=1}^{i-1} \left(\frac{a_j^2}{2} + \frac{\varepsilon_j^2}{2} + \frac{\bar{d}_j^2}{2} \right). \quad (3.18)$$

By incorporating (3.16) into (3.15), one has

$$\begin{aligned} \dot{V}_i \leq & -\sum_{j=1}^{i-1} k_j e_j^2 + e_{i-1}e_i + \sum_{j=1}^{i-1} \frac{1}{r_j} \delta_j \tilde{\theta}_j \hat{\theta}_j + \sum_{j=1}^{i-1} \left(\frac{a_j^2}{2} + \frac{\varepsilon_j^2}{2} + \frac{\bar{d}_j^2}{2} \right) + z_i(\bar{f}_i(X_i) + e_{i+1} + d_i(t) + \alpha_i) \\ & - \frac{1}{r_i} \tilde{\theta}_i \dot{\hat{\theta}}_i - \frac{1}{2} e_i^2, \end{aligned} \quad (3.19)$$

where $\bar{f}_i(X_i) = f_i(x) - \dot{\alpha}_{i-1} + \frac{1}{2}e_i$. The function $\bar{f}_i(X_i)$ involves the unknown smooth function f_i . Consequently, the RBFNN $W_i^{*T} S_i(X_i)$ is utilized to approximate the unknown function $\bar{f}_i(X_i)$, ensuring that, for any positive $\varepsilon_i > 0$,

$$\bar{f}_i(X_i) = W_i^{*T} S_i(X_i) + \delta_i(X_i), \quad |\delta_i(X_i)| < \varepsilon_i, \quad (3.20)$$

where $X_i = [x_1, \dots, x_n, \hat{\theta}_1, \dots, \hat{\theta}_{i-1}, \lambda_1, \dots, \lambda_i]^T$.

Applying a similar approach as in (3.6), one has

$$e_i \bar{f}_i \leq \frac{1}{2a_i^2} z_i^2 \theta_i S_i^T(Z_i) S_i(Z_i) + \frac{a_i^2}{2} + \frac{e_i^2}{2} + \frac{\varepsilon_i^2}{2}, \quad (3.21)$$

where $Z_i = [x_1, \dots, x_i, \hat{\theta}_1, \dots, \hat{\theta}_{i-1}]^T$, $\theta_i = \|W_i^*\|^2$, and $a_i > 0$ is a design parameter.

Applying Young's inequality, we have

$$e_i d_i(t) \leq \frac{e_i^2}{2} + \frac{\bar{d}_i^2}{2}, \quad (3.22)$$

where $\bar{d}_i > 0$ is a constant.

The virtual control input signal α_i can be selected as follows:

$$\alpha_i = -k_i e_i - e_{i-1} - \frac{1}{2a_i^2} e_i \hat{\theta}_i S_i^T(Z_i) S_i(Z_i), \quad (3.23)$$

where k_i and a_i are positive design constants.

By using Lemma 2.2 and (3.23), one has

$$e_i \alpha_i \leq -k_i e_i^2 - \frac{1}{2a_i^2} e_i^2 \hat{\theta}_i S_i^T(Z_i) S_i(Z_i). \quad (3.24)$$

By incorporating (3.21)–(3.24) into (3.19), we have

$$\begin{aligned} \dot{V}_i \leq & - \sum_{j=1}^i k_j e_j^2 + e_{i+1} e_i + \sum_{j=1}^{i-1} \frac{1}{r_j} \vartheta_j \tilde{\theta}_j \hat{\theta}_j + \sum_{j=1}^i \left(\frac{a_j^2}{2} + \frac{\varepsilon_j^2}{2} + \frac{\bar{d}_j^2}{2} \right) \\ & + \left(\frac{1}{2a_i^2} e_i^2 S_i^T(Z_i) S_i(Z_i) \right) (\theta_i - \hat{\theta}_i) - \frac{1}{r_i} \tilde{\theta}_i \hat{\theta}_i. \end{aligned} \quad (3.25)$$

Given that $\tilde{\theta}_i = \theta_i - \hat{\theta}_i$, (3.25) becomes

$$\begin{aligned} \dot{V}_i \leq & - \sum_{j=1}^i k_j e_j^2 + e_{i+1} e_i + \sum_{j=1}^{i-1} \frac{1}{r_j} \vartheta_j \tilde{\theta}_j \hat{\theta}_j + \sum_{j=1}^i \left(\frac{a_j^2}{2} + \frac{\varepsilon_j^2}{2} + \frac{\bar{d}_j^2}{2} \right) \\ & + \frac{1}{r_1} \tilde{\theta}_i \left(\frac{1}{2a_i^2} r_i e_i^2 S_i^T(Z_i) S_i(Z_i) - \hat{\theta}_i \right). \end{aligned} \quad (3.26)$$

The adaptive law $\dot{\hat{\theta}}_i$ can be selected as follows:

$$\dot{\hat{\theta}}_i = \frac{r_i}{2a_i^2} e_i^2 S_i^T(Z_i) S_i(Z_i) - \vartheta_i \hat{\theta}_i, \quad (3.27)$$

where r_i and ϑ_i are positive design constants.

Moreover, by substituting (3.27) into (3.26), one has

$$\dot{V}_i \leq - \sum_{j=1}^i k_j e_j^2 + e_{i+1} e_i + \sum_{j=1}^{i-1} \frac{1}{r_j} \vartheta_j \tilde{\theta}_j \hat{\theta}_j + \sum_{j=1}^i \left(\frac{a_j^2}{2} + \frac{\varepsilon_j^2}{2} + \frac{\bar{d}_j^2}{2} \right). \quad (3.28)$$

Step n . According to (3.1) and (2.7), the time derivative of e_n is given by

$$\dot{e}_n = \dot{x}_n - \dot{\alpha}_{n-1} = f_n(x_n) + x_{n+1} - \lambda(t, t_\lambda) v - u_r(t, t_r) + d_n(t) - \dot{\alpha}_{n-1} + \frac{\dot{x}_{n+1}}{\rho}, \quad (3.29)$$

where α_{n-1} is defined as follows:

$$\dot{\alpha}_{n-1} = \sum_{j=0}^{n-1} \frac{\partial \alpha_{n-1}}{\partial y_d^{(j)}} y_r^{(j+1)} + \sum_{j=1}^{n-1} \frac{\partial \alpha_{n-1}}{\partial x_j} (f_j(x) + x_{j+1} + d_j(t)) + \sum_{j=1}^{n-1} \frac{\partial \alpha_{n-1}}{\partial \theta_j} \dot{\theta}_j. \quad (3.30)$$

Take the Lyapunov function as follows:

$$V_n = V_{n-1} + \frac{1}{2} e_n^2 + \frac{1}{2r_n} \tilde{\theta}_n^2, \quad (3.31)$$

where $\tilde{\theta}_n = \theta_n - \hat{\theta}_n$ represents the estimation error and $r_n > 0$ represents the design constant.

Further, the dynamics of V_n are given by

$$\begin{aligned}
 \dot{V}_n &\leq \dot{V}_{n-1} + e_n \left(f_n(x_n) + x_{n+1} - \lambda(t, t_\lambda)v - u_r(t, t_r) + d_n(t) - \dot{\alpha}_{n-1} + \frac{-\rho x_{n+1}}{\rho} \right. \\
 &\quad \left. + \frac{2\rho\lambda(t, t_\lambda)v}{\rho} + \frac{2\rho u_r(t, t_r)}{\rho} \right) - \frac{1}{r_n} \tilde{\theta}_n \dot{\hat{\theta}}_n \\
 &\leq \dot{V}_{n-1} + e_n \left(f_n(x_n) + x_{n+1} - \lambda(t, t_\lambda)v - u_r(t, t_r) + d_n(t) - \dot{\alpha}_{n-1} - x_{n+1} \right. \\
 &\quad \left. + 2\lambda(t, t_\lambda)v + 2u_r(t, t_r) \right) - \frac{1}{r_n} \tilde{\theta}_n \dot{\hat{\theta}}_n \\
 &\leq \dot{V}_{n-1} + e_n \left(f_n(x_n) + \lambda(t, t_\lambda)v + u_r(t, t_r) + d_n(t) - \dot{\alpha}_{n-1} \right) - \frac{1}{r_n} \tilde{\theta}_n \dot{\hat{\theta}}_n.
 \end{aligned} \tag{3.32}$$

The derivative of V_{n-1} is given as follows:

$$\dot{V}_{n-1} \leq - \sum_{j=1}^{n-1} k_j e_j^2 + \sum_{j=1}^{n-1} \frac{1}{r_j} \vartheta_j \tilde{\theta}_j \hat{\theta}_j + \sum_{j=1}^{n-1} \left(\frac{a_j^2}{2} + \frac{\varepsilon_j^2}{2} + \frac{\bar{d}_j^2}{2} \right). \tag{3.33}$$

By incorporating (3.29) into (3.28), one has

$$\begin{aligned}
 \dot{V}_n &\leq - \sum_{j=1}^{n-1} k_j e_j^2 + \sum_{j=1}^{n-1} \frac{1}{r_j} \delta_j \tilde{\theta}_j \hat{\theta}_j + \sum_{j=1}^{n-1} \left(\frac{a_j^2}{2} + \frac{\varepsilon_j^2}{2} + \frac{\bar{d}_j^2}{2} \right) + e_n \left(\bar{f}_n(X_n) + \lambda(t, t_\lambda)v + u_r(t, t_r) + d_n(t) \right) \\
 &\quad - \frac{1}{r_n} \tilde{\theta}_n \dot{\hat{\theta}}_n - \frac{1}{2} e_n^2,
 \end{aligned} \tag{3.34}$$

where $\bar{f}_n(X_n) = f_n(x) - \dot{\alpha}_{n-1} + \frac{1}{2}e_n$. The function $\bar{f}_n(X_n)$ involves the unknown smooth function f_n . Therefore, the RBFNN $W_n^{*T} S_n(X_n)$ is employed to estimate the unknown function $\bar{f}_n(X_n)$, ensuring that, for any positive $\varepsilon_n > 0$,

$$\bar{f}_n(X_n) = W_n^{*T} S_n(X_n) + \delta_n(X_n), \quad |\delta_n(X_n)| < \varepsilon_n, \tag{3.35}$$

where $X_n = [x_1, \dots, x_n, \hat{\theta}_1, \dots, \hat{\theta}_{n-1}]^T$.

Applying a similar approach as in (3.6), one has

$$e_n \bar{f}_n \leq \frac{1}{2a_n^2} z_n^2 \theta_n S_n^T(Z_n) S_n(Z_n) + \frac{a_n^2}{2} + \frac{e_n^2}{2} + \frac{\varepsilon_n^2}{2}, \tag{3.36}$$

where $Z_n = [x_1, \dots, x_n, \hat{\theta}_1, \dots, \hat{\theta}_{n-1}]^T$, $\theta_n = \|W_n^*\|^2$, and $a_n > 0$ is a design parameter.

Applying Young's inequality, we have

$$e_n d_n(t) \leq \frac{e_n^2}{2} + \frac{\bar{d}_n^2}{2}, \tag{3.37}$$

where $\bar{d}_n > 0$ is a constant.

Utilizing Lemma 2.2 and considering Assumption 2.2, we have

$$e_n u_r(t, t_r) \leq \frac{e_n^2}{2} + \frac{u_{\max}^2}{2}. \tag{3.38}$$

The real control law v can be selected as follows:

$$v = -k_n e_n - e_{n-1} - \frac{1}{2a_n^2} e_n \hat{\theta}_n S_n^T(Z_n) S_n(Z_n), \quad (3.39)$$

where k_n and a_n are positive design constants.

By using Lemma 2.2, Assumption 2.2 and (3.39), one has

$$e_n v \leq -k_n \lambda_{\min} e_n^2 - e_n e_{n-1} - \frac{1}{2a_n^2} e_n^2 \hat{\theta}_n S_n^T(Z_n) S_n(Z_n). \quad (3.40)$$

By incorporating (3.36)–(3.40) into (3.34), we have

$$\begin{aligned} \dot{V}_i \leq & - \sum_{j=1}^{n-1} k_j e_j^2 - k_n \lambda_{\min} e_n^2 + \sum_{j=1}^{i-1} \frac{1}{r_j} \vartheta_j \tilde{\theta}_j \hat{\theta}_j + \sum_{j=1}^i \left(\frac{a_j^2}{2} + \frac{\varepsilon_j^2}{2} + \frac{\bar{d}_j^2}{2} \right) + \frac{u_{\max}^2}{2} \\ & + \left(\frac{1}{2a_n^2} e_n^2 S_n^T(Z_n) S_n(Z_n) \right) (\theta_n - \hat{\theta}_n) - \frac{1}{r_n} \tilde{\theta}_n \dot{\hat{\theta}}_n. \end{aligned} \quad (3.41)$$

Given that $\tilde{\theta}_n = \theta_n - \hat{\theta}_n$, (3.41) becomes

$$\begin{aligned} \dot{V}_n \leq & - \sum_{j=1}^{n-1} k_j e_j^2 - k_n \lambda_{\min} e_n^2 + \sum_{j=1}^{n-1} \frac{1}{r_j} \vartheta_j \tilde{\theta}_j \hat{\theta}_j + \sum_{j=1}^n \left(\frac{a_j^2}{2} + \frac{\varepsilon_j^2}{2} + \frac{\bar{d}_j^2}{2} \right) + \frac{u_{\max}^2}{2} \\ & + \frac{1}{r_n} \tilde{\theta}_n \left(\frac{1}{2a_n^2} r_n e_n^2 S_n^T(Z_n) S_n(Z_n) - \dot{\hat{\theta}}_n \right). \end{aligned} \quad (3.42)$$

The adaptive law $\dot{\hat{\theta}}_n$ can be selected as follows:

$$\dot{\hat{\theta}}_n = \frac{r_n}{2a_n^2} e_n^2 S_n^T(Z_n) S_n(Z_n) - \vartheta_n \hat{\theta}_n, \quad (3.43)$$

where r_n and ϑ_n are positive design constants.

Furthermore, it results from substituting (3.43) into (3.42) and applying Assumption 2.2 that

$$\dot{V}_n \leq - \sum_{j=1}^{n-1} k_j e_j^2 - k_n \lambda_{\min} e_n^2 + \sum_{j=1}^n \frac{1}{r_j} \vartheta_j \tilde{\theta}_j \hat{\theta}_j + \sum_{j=1}^n \left(\frac{a_j^2}{2} + \frac{\varepsilon_j^2}{2} + \frac{\bar{d}_j^2}{2} \right) + \frac{u_{\max}^2}{2}. \quad (3.44)$$

Theorem 3.1. Consider the nonstrict feedback nonlinear system (2.1) with input delay and actuator faults under Assumptions 2.1 and 2.2, the real controller (3.39), the virtual control laws (3.8) and (3.23), and the adaptive laws (3.12), (3.27) and (3.43). The presented control scheme guarantees the achievement of the following control objectives: (1) The SGUUB nature of all variables within the closed-loop system. (2) The convergence of the system's tracking error to a compact region around the origin.

Proof. By studying the definition of $\tilde{\theta}_j$, one has

$$\tilde{\theta}_j \hat{\theta}_j \leq \theta_j^2 - \tilde{\theta}_j^2. \quad (3.45)$$

By substituting (3.45) into (3.44), we have

$$\begin{aligned}
 \dot{V}_n &\leq -\sum_{j=1}^{n-1} k_j e_j^2 + k_n \lambda_{\min} e_n^2 + \sum_{j=1}^n \frac{1}{r_j} \vartheta_j \theta_j^2 - \sum_{j=1}^n \frac{1}{r_j} \vartheta_j \tilde{\theta}_j^2 + \sum_{j=1}^n \left(\frac{a_j^2}{2} + \frac{\epsilon_j^2}{2} + \frac{\bar{d}_j^2}{2} \right) + \frac{u_{\max}^2}{2} \\
 &= -\sum_{j=1}^{n-1} k_j e_j^2 + k_n \lambda_{\min} e_n^2 - \sum_{j=1}^n \frac{1}{r_j} \vartheta_j \tilde{\theta}_j^2 + \sum_{j=1}^n \left(\frac{1}{r_j} \vartheta_j \theta_j^2 + \frac{a_j^2}{2} + \frac{\epsilon_j^2}{2} + \frac{\bar{d}_j^2}{2} \right) + \frac{u_{\max}^2}{2} \\
 &\leq -a_0 \sum_{j=1}^n \left(\frac{1}{2} e_j^2 + \frac{1}{2r_j} \tilde{\theta}_j^2 \right) + b_0 \\
 &\leq -a_0 V_n + b_0,
 \end{aligned} \tag{3.46}$$

where $a_0 = 2m$, $m = \min\{k_1, \dots, k_n \lambda_{\min}, \vartheta_1, \dots, \vartheta_n\}$, and $b_0 = \sum_{j=1}^n \left(\frac{\vartheta_j \theta_j^2}{r_j} + \frac{a_j^2}{2} + \frac{\epsilon_j^2}{2} + \frac{\bar{d}_j^2}{2} \right) + \frac{u_{\max}^2}{2}$.

Integrating (3.46) over the interval $[0, t]$, we can derive the following inequality:

$$V_n(t) \leq V_n(0)e^{-a_0 t} + \frac{b_0}{a_0}(1 - e^{-a_0 t}). \tag{3.47}$$

Considering the definition of V_n in (3.31) and the inequality (3.47), it can be inferred that e_i ($i = 1, \dots, n$) and θ_i ($i = 1, \dots, n$) are bounded. Taking $e_1 = x_1 - y_d$ and the boundedness of e_1 and y_d into account, it implies that the state x_1 is bounded. For $e_i = x_i - \alpha_{i-1}$ and the definition of the virtual control signal α_i ($i = 1, \dots, n-1$) along with Assumption 2.1, it can be concluded that x_i ($i = 2, \dots, n$) remains bounded. Additionally, from (3.39), it can be deduced that the control v is also bounded. Therefore, all signals in the closed-loop system are SGUUB. Moreover, based on (3.47), one has

$$e_1^2 \leq 2 \left(V(0) - \frac{b_0}{a_0} \right) e^{-a_0 t} + \frac{b_0}{a_0}. \tag{3.48}$$

Hence, the proof is completed.

Figure 1 depicts the architecture of the control scheme that is being discussed.

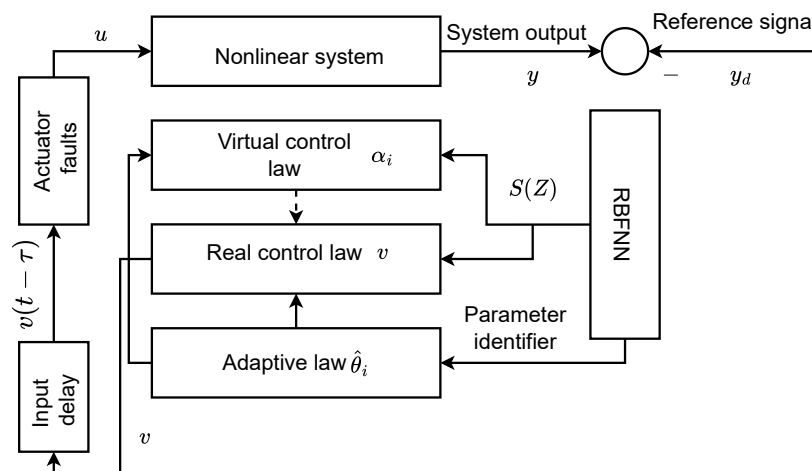


Figure 1. Architecture of control system.

Remark 3.1. Improved tracking performance is achievable by reducing the IC values. However, it is crucial to carefully select the appropriate ascertained. Furthermore, as can be ascertained from (3.46), the tracking error decreases as the parameters k_i , ϑ_i increase and b_i decreases. It is important to keep in mind that selecting a sufficiently high value for k_i and ϑ_i results in a larger control energy. Typically, both initial conditions and design parameters are determined through a trial-and-error method, where system performance is observed and adjustments are made accordingly. Therefore, it is essential to design the parameters appropriately in real-world engineering settings to achieve improved transient performance and efficient control action while avoiding excess control energy.

4. Simulation results

In this section, the efficacy of the presented control schemes will be assessed through the two examples. The methodology outlined in Theorem 3.1 will be employed to formulate controllers to regulate the considered systems.

Example 4.1. Consider the following nonstrict-feedback nonlinear system:

$$\begin{cases} \dot{x}_1 = x_2 + 1 - \cos(x_1 x_3) + x_3 + x_2 + 0.5 \cos(t), \\ \dot{x}_2 = x_3 + x_1^2 x_3 e^{-x_2^2} + \sin(0.5t), \\ \dot{x}_3 = u(v(t - \tau)) + x_1 x_2^2 e^{-x_3^2} + x_3 \sin(x_1 x_2), \\ y = x_1, \end{cases} \quad (4.1)$$

where $f_1(x) = 1 - \cos(x_1 x_3) + x_3 + x_2$, $f_2(x) = x_1^2 x_3 e^{-x_2^2}$, $f_3(x) = x_1 x_2^2 e^{-x_3^2} + x_3 \sin(x_1 x_2)$, $d_1(t) = 0.5 \cos(t)$, $d_2(t) = \sin(0.5t)$, $d_3(t) = 0$, $\tau = 1.5s$.

The reference signal was set as $y_d = 0.5(\sin(t) + 0.5 \sin(0.5t))$. The system input subject to actuator fault described by $u(v(t)) = \lambda(t, t_\lambda)v + u_r(t, t_r)$ with $\lambda(t, t_\lambda) = 0.4 + 0.6 \exp(-0.2t)$, and $u_r(t, t_r) = \cos^2(x_1)x_2$. The following virtual control laws, real control law and, adaption laws are considered:

$$\begin{aligned} \alpha_i &= -k_i e_i - e_{i-1} - \frac{1}{2a_i^2} e_i \hat{\theta}_i S_i^T(Z_i) S_i(Z_i), \quad i = 1, 2. \\ v &= -k_3 e_3 - e_2 - \frac{1}{2a_3^2} e_3 \hat{\theta}_3 S_3^T(Z_3) S_3(Z_3), \\ \hat{\theta}_i &= \frac{r_i}{2a_i^2} e_i^2 S_i^T(Z_i) S_i(Z_i) - \vartheta_i \hat{\theta}_i, \quad i = 1, 2, 3. \end{aligned} \quad (4.2)$$

The center of the receptive field was chosen as $\mu_i = [-1.5, -1, -0.5, 0, 0.5, 1, 1.5]^T$ for $i = 1, 2, 3$, and the Gaussian function's width was set to $\zeta = 2$. In the simulation, the design parameters were determined using the trial-and-error method, as follows: $k_1 = k_2 = 3$, $k_3 = 6$, $a_1 = a_2 = a_3 = 3$, $\vartheta_1 = 1$, $\vartheta_2 = 1$, $\vartheta_3 = 1$, $r_1 = 1$, $r_2 = 1$, $r_3 = 1$. The simulation began with ICs set via the trial-and-error method as $[x_1(0), x_2(0), x_3(0)]^T = [0.5, 0.5, 0.5]^T$ and $[\hat{\theta}_1(0), \hat{\theta}_2(0), \hat{\theta}_3(0)] = [0, 0, 0]$.

The simulation results are depicted in Figures 2–7. Figure 2 illustrates the trajectories of the system output $y = x_1$ and the reference signal y_d . As observed in Figure 2, the output $y = x_1$ adeptly tracks the reference signal y_d with bounded error, and the tracking error e_1 is depicted in Figure 3. The trajectories of x_2 and x_3 are presented in Figure 4. Figure 5 showcases the bounded adaptive laws $\hat{\theta}_1$, $\hat{\theta}_2$, and $\hat{\theta}_3$,

while Figure 6 displays the control input v and system input u . The simulation results affirm that the proposed controller ensures the boundedness of all signals within the closed-loop system.

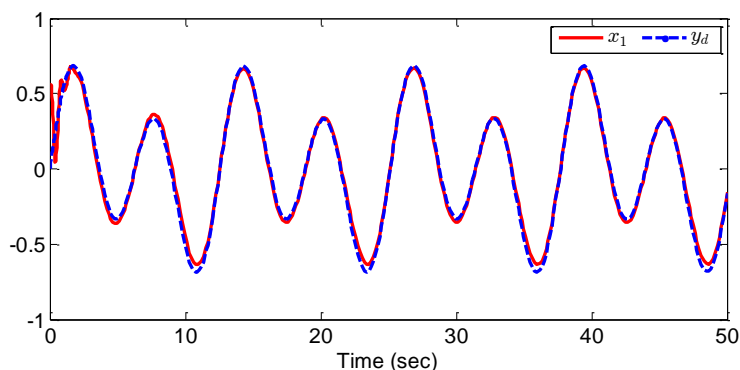


Figure 2. The trajectories of x_1 and y_d .

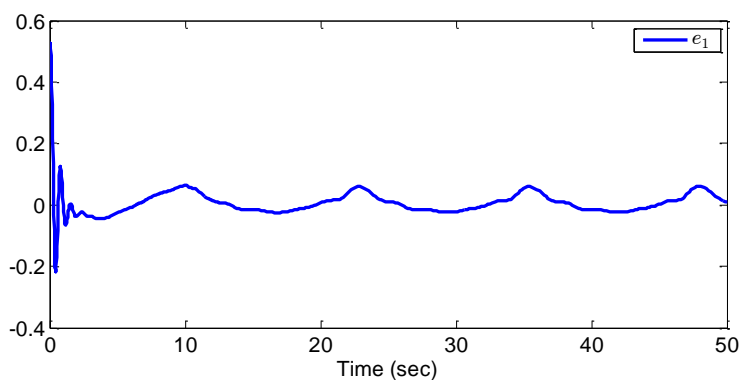


Figure 3. The trajectory of tracking error e_1 .

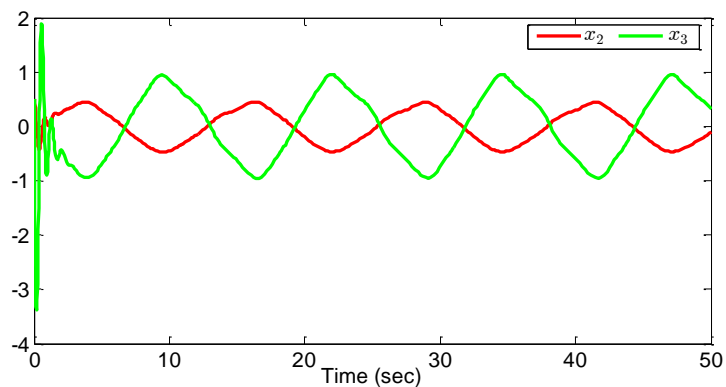


Figure 4. The trajectories of system states x_2 and x_3 .

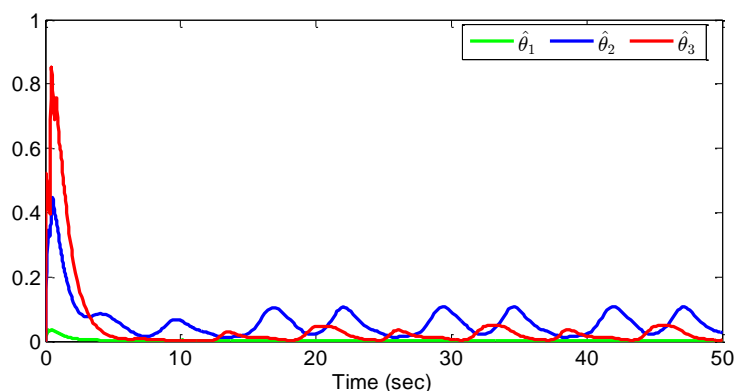


Figure 5. The trajectories of adaptive laws $\hat{\theta}_1$, $\hat{\theta}_2$, and $\hat{\theta}_3$.

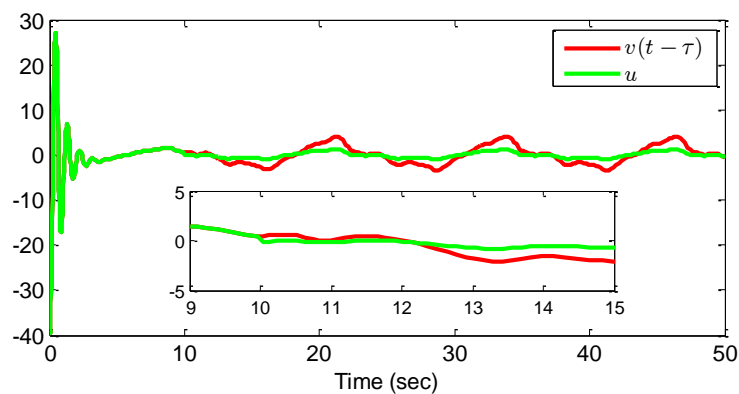


Figure 6. Real control law $v(t - \tau)$ and system input u .

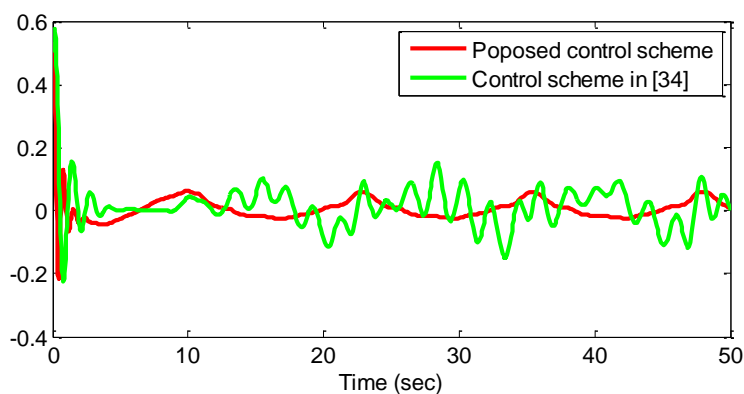


Figure 7. Tracking error e_1 .

In this study, the effectiveness of the proposed method was validated through a comparison with an existing control approach [29] that utilizes auxiliary systems to minimize the effects of input delay. In contrast to the established control method, the proposed approach integrates Pade approximation. The

comparison results, illustrated in Figure 7, clearly demonstrate a slight yet consistent improvement in tracking error under the proposed control method relative to the existing approach [29].

Figures 2–7 collectively highlight that, through judicious parameter adjustments, the designed controller effectively constrains all closed-loop system signals. This validation demonstrates the effectiveness of the proposed controller.

Moreover, error assessment criteria [33] were employed to substantiate the effectiveness of the proposed method in comparison to the existing approach [29]. For a given pair of data points $(y_i(t), y_{id}(t))$ in the interval $t \in [1, P]$ with P as the observations in the data set, the assessment error criteria were as follows:

$$\begin{aligned} \text{Mean squared error (MSE):} &= \frac{\sum_{t=1}^P (y_i(t) - y_{id})^2}{P}; \\ \text{Root mean squared error (RMSE):} &= \sqrt{\frac{1}{P} \sum_{t=1}^P (y_i(t) - y_{id}(t))^2}; \\ \text{Maximum absolute error (MAE):} &= \max_{1 \leq t \leq P} |y_i(t) - y_{id}(t)|; \\ \text{Normalized mean squared error (NMSE):} &= \frac{\sum_{t=1}^P (y_i(t) - y_{id}(t))^2}{\sum_{t=1}^P (y_i(t) - \bar{y}_{id})^2}; \\ \text{Sum of squared error (SSE):} &= \sum_{t=1}^P (y_i(t) - y_{id}(t))^2; \\ \text{Best fit rate (BFR):} &= 1 - \frac{\sum_{t=1}^P (y_i(t) - y_{id}(t))^2}{\sum_{t=1}^P (y_i(t) - \bar{y}_{id})^2} \times 100\%, \end{aligned}$$

where \bar{y}_{id} represents the mean of $y_{id}(t)$.

The results, as depicted in Table 1, demonstrate a marginal improvement in the proposed control scheme relative to the existing control method [29]. This enhancement provides compelling evidence of the effectiveness of the proposed control approach.

Table 1. Comparison of the tracking performance based on different error calculations.

Methods	MSE	RMSE	MAE	NMSE	SSE	BFR
Proposed method	0.0160	0.1266	0.5375	0.0998	6.6997	99.90%
Existing method in [29]	0.0171	0.1307	0.5187	0.1045	8.2522	99.90%

Remark 4.1. Understanding the convergence dynamics of the system components is largely dependent on the time constant and half-life analyses. In Figure 2, the modest convergence speed for x_1 is indicated by a time constant of 19.6239 seconds, indicating that it takes about 0.3651 seconds to reach half of its initial value. In Figure 3, a longer time constant of 32.6245 seconds is shown by the tracking error (e_1), which suggests a slower rate of convergence with a half-life of roughly 0.2685 seconds. In Figure 5, $\hat{\theta}_1$, $\hat{\theta}_2$, and $\hat{\theta}_3$ are shown to have time constants of 121.8149 seconds, 11.4806 seconds, and 2.8463 seconds in that ratio. Additionally, the half-life of 0.0000 seconds that was consistently reported for each parameter points to nuances in their convergence dynamics that are not explained by the conventional half-life criterion of attaining half of the initial value.

Example 4.2. To further illustrate the effectiveness of the proposed method, the electromechanical system in [34] was employed. It is governed by the following dynamic equations:

$$\begin{cases} M\ddot{q} + B\dot{q} + N \sin(q) = I, \\ LI = V_\epsilon - RI - K_B\dot{q}, \end{cases} \quad (4.3)$$

where

$$\begin{aligned} M &= \frac{J}{K_t} + \frac{mL_0^2}{3K_t} + \frac{2M_0R_0^2}{5K_t}, \\ N &= \frac{mL_0G}{2K_t} + \frac{M_0L_0G}{K_t}, \\ B &= \frac{B_0}{K_t}, \end{aligned}$$

and \ddot{q} , \dot{q} , q stand for the link acceleration, velocity, and position, respectively. V_ϵ represents the input. $J = 0.001625$, $K_t = 0.9$, $m = 0.506$, $L_0 = 0.305$, $M_0 = 0.434$, $R_0 = 0.023$, $G = 9.8$, and $B_0 = 0.01625$. The physical meaning of the electromechanical system can be found in [34]. Defining $x_1 = q$, $x_2 = \dot{q}$, $x_3 = I$, and $u(v(t - \tau)) = V_\epsilon$, the (4.3) can be rewritten as follows:

$$\begin{cases} \dot{x}_1 = x_2 + 0.2 \sin(t), \\ \dot{x}_2 = \frac{x_3}{M} - \frac{N}{M} \sin x_1 - \frac{B}{M} x_2 + \frac{B}{M} \cos x_2 \sin x_3, \\ \dot{x}_3 = \frac{u(v(t-\tau))}{L} - \frac{K}{L} x_2 - \frac{R}{L} x_3 + \sin(2t), \\ y = x_1, \end{cases} \quad (4.4)$$

where $f_1(x) = 0$, $f_2(x) = -\frac{N}{M} \sin x_1 - \frac{B}{M} x_2 + \frac{B}{M} \cos x_2 \sin x_3$, $f_3(x) = -\frac{K}{L} x_2 - \frac{R}{L} x_3$, $d_1(t) = 0.2 \sin(t)$, $d_2(t) = 0$, $d_3(t) = \sin(2t)$, $\tau = 1.5s$.

The reference signal is set as $y_d = 0.5 \sin(t) - \cos(0.5t)$. The system input subject to actuator fault described by $u(v(t)) = \lambda(t, t_\lambda)v + u_r(t, t_r)$ with $\lambda(t, t_\lambda) = 0.4 + 0.6 \exp(-0.2t)$, and $u_r(t, t_r) = \cos^2(x_1)x_2$. The following virtual control laws, real control law and adaption laws are considered:

$$\begin{aligned} \alpha_i &= -k_i e_i - e_{i-1} - \frac{1}{2a_i^2} e_i \hat{\theta}_i S_i^T(Z_i) S_i(Z_i), \quad i = 1, 2. \\ v &= -k_3 e_3 - e_2 - \frac{1}{2a_3^2} e_3 \hat{\theta}_3 S_3^T(Z_3) S_3(Z_3), \\ \hat{\theta}_i &= \frac{r_i}{2a_i^2} e_i^2 S_i^T(Z_i) S_i(Z_i) - \vartheta_i \hat{\theta}_i, \quad i = 1, 2, 3. \end{aligned} \quad (4.5)$$

The receptive field center is defined as $\mu_i = [-1.5, -1, -0.5, 0, 0.5, 1, 1.5]^T$ for $i = 1, 2, 3$, with a Gaussian function width of $\zeta = 2$. In the simulation, design parameters are determined through the trial-and-error method: $k_1 = 8$, $k_2 = 7$, $k_3 = 8$, $a_1 = a_2 = a_3 = 1$, $\vartheta_1 = 1$, $\vartheta_2 = 1$, $\vartheta_3 = 1$, $r_1 = 1$, $r_2 = 1$, $r_3 = 1$. ICs for the simulation are set by using the trial-and-error method: $[x_1(0), x_2(0), x_3(0)]^T = [0.5, 0.5, -0.5]^T$ and $[\hat{\theta}_1(0), \hat{\theta}_2(0), \hat{\theta}_3(0)] = [0, 0, 0]$.

The simulation outcomes are displayed in Figures 8–13. Figure 8 demonstrates the effective tracking of the output $y = x_1$ to the reference signal y_d with bounded error. Further insights into

the tracking error e_1 are provided in Figure 9. Trajectories of x_2 and x_3 are depicted in Figure 10. Figure 11 presents the bounded adaptive laws $\hat{\theta}_1$, $\hat{\theta}_2$, and $\hat{\theta}_3$, while Figure 12 exhibits the control input v and system input u .

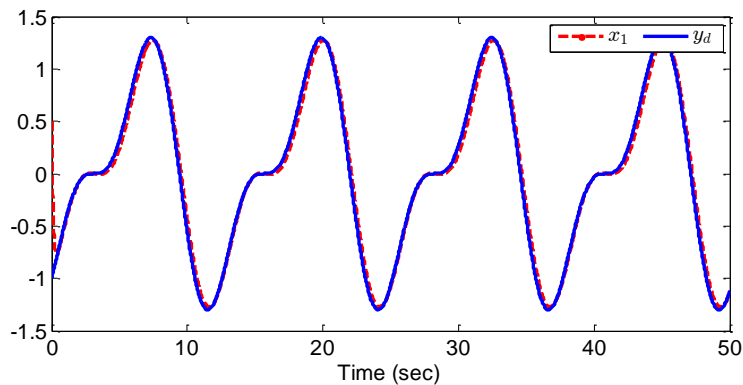


Figure 8. The trajectories of x_1 and y_d .

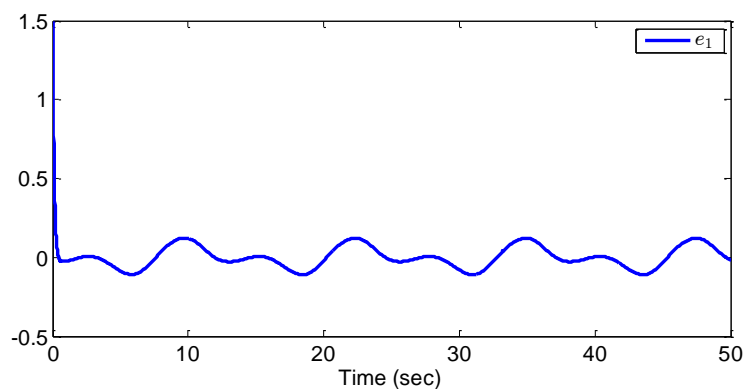


Figure 9. The trajectory of tracking error e_1 .

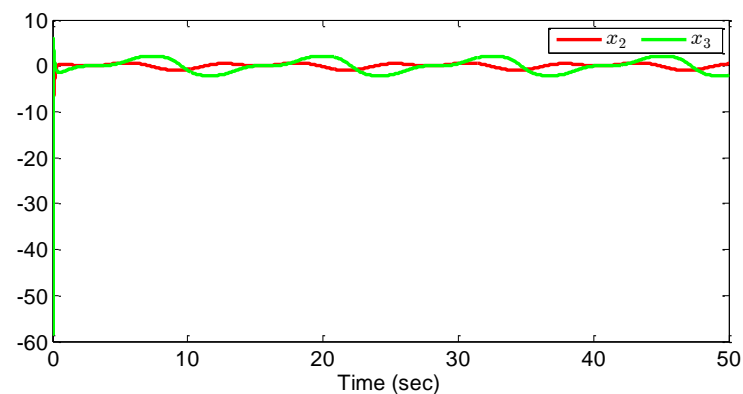


Figure 10. Trajectories of system states x_2 and x_3 .

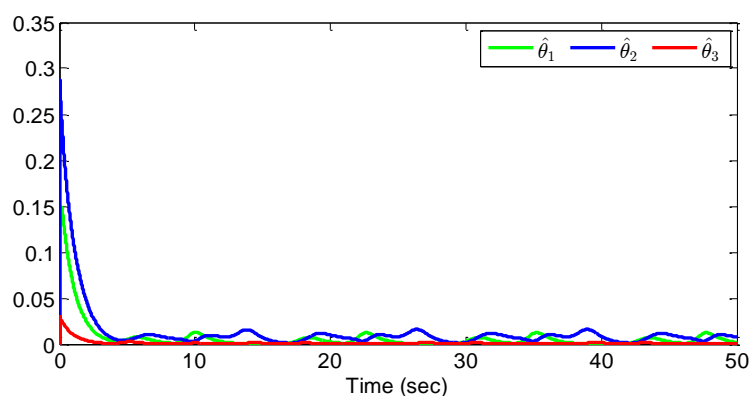


Figure 11. The trajectories of adaptive laws $\hat{\theta}_1$, $\hat{\theta}_2$, and $\hat{\theta}_3$.

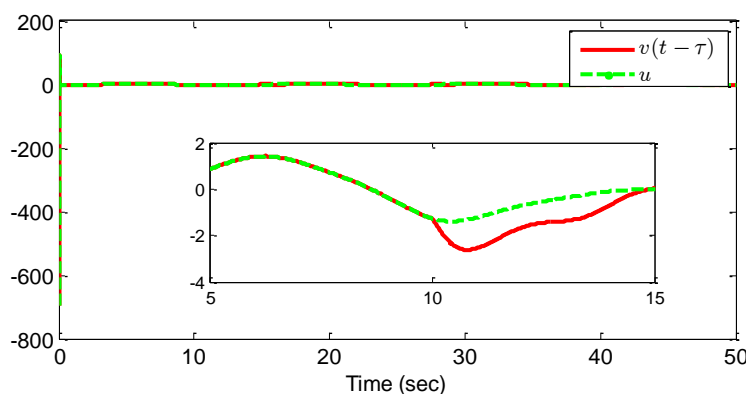


Figure 12. Real control law $v(t - \tau)$ and system input u .

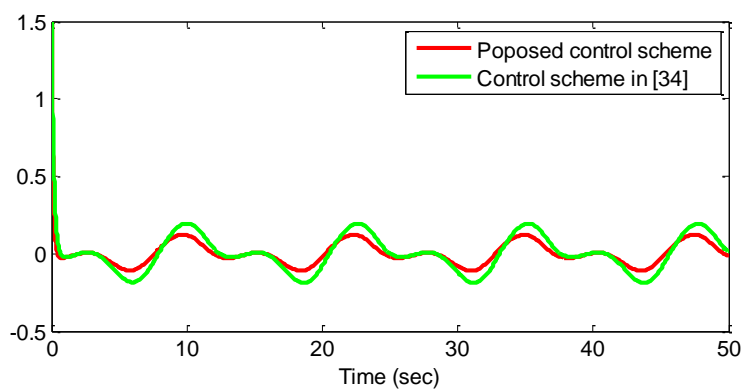


Figure 13. Tracking error e_1 .

In this study, the effectiveness of the proposed method was validated through a comparison with an existing control approach [29] that utilizes auxiliary systems to minimize the effects of input delay. In contrast to the established control method, the proposed approach integrates Pade approximation. The comparison results, illustrated in Figure 13, clearly demonstrate a slight yet consistent improvement in

tracking error under the proposed control method relative to the existing approach [29]. The simulation results affirm that the proposed controller ensures the boundedness of all signals within the closed-loop system. Figures 8–13 collectively highlight that, through judicious parameter adjustments, the designed controller effectively constrains all closed-loop system signals. This validation demonstrates the effectiveness of the proposed controller.

In this illustrative example, the error assessment criteria defined in Example 4.1 were utilized to establish the effectiveness of the proposed method as compared to the existing approach [29].

The results, as depicted in Table 2, demonstrate a marginal improvement in the proposed control scheme relative to the existing control method [29]. This enhancement provides compelling evidence of the effectiveness of the proposed control approach.

Table 2. Comparison of the tracking performance for different error calculations.

Methods	MSE	RMSE	MAE	NMSE	SSE	BFR
Proposed method	0.0287	0.1695	1.5000	0.0590	119.8038	99.94%
Existing method in [29]	0.0417	0.2042	1.5000	0.0970	136.1849	99.90%

Remark 4.2. Comprehending the convergence dynamics of system elements heavily relies on the examination of time constants and half-life analyses. In Figure 8, the relatively moderate pace at which x_1 converges is indicated by a time constant of 2.6835 seconds, and it took about 0.0504 seconds to become half of its initial value. In Figure 9, the tracking error (e_1) demonstrates a lengthier time constant of 11.8472 seconds, suggesting a slower convergence rate with a half-life of approximately 0.1387 seconds. In Figure 11, $\hat{\theta}_1$, $\hat{\theta}_2$, and $\hat{\theta}_3$ have time constants of 23.7414 seconds, 3.7447 seconds, and 1.2005 seconds, respectively. Moreover, the consistently reported half-life of 0.0000 seconds for each parameter underscores intricacies in their convergence dynamics that are not fully explicable by the conventional half-life criterion associated with achieving half of the initial value.

5. Conclusions

The adaptive control problem for nonstrict-feedback nonlinear systems with actuator faults, input delays, and external disturbances has been the primary focus of this study. The use of an RBFNN and the Padé approximation, respectively, helped to resolve the difficulties brought forth by input delay and unknown functions. An adaptive controller has been developed by applying the Lyapunov stability theorem with the backstepping approach. The tracking error of the suggested controller converges to a small neighborhood around the origin, guaranteeing the boundedness of all signals in the closed-loop system. The efficacy of the suggested control method has been confirmed by the simulation results. Future research will concentrate on nonlinear systems with sensors and actuator faults, including providing true and estimated values of the nonlinear function to improve overall performance.

Use of AI tools declaration

The authors declare they have not used Artificial Intelligence (AI) tools in the creation of this article.

Acknowledgments

This work was funded by the Princess Nourah bint Abdulrahman University Researchers Supporting Project number (PNURSP2024R528), Princess Nourah bint Abdulrahman University, Riyadh, Saudi Arabia.

Conflict of interest

The authors confirm no conflicts of interest.

References

1. H. Q. Wang, H. R. Karimi, P. X. Liu, H. Yang, Adaptive neural control of nonlinear systems with unknown control directions and input dead-zone, *IEEE Trans. Syst. Man Cybern. Syst.*, **48** (2018), 1897–1907. <https://doi.org/10.1109/TSMC.2017.2709813>
2. D. S. Yang, T. Li, X. P. Xie, H. G. Zhang, Event-triggered integral sliding-mode control for nonlinear constrained-input systems with disturbances via adaptive dynamic programming, *IEEE Trans. Syst. Man Cybern. Syst.*, **50** (2020), 4086–4096. <https://doi.org/10.1109/TSMC.2019.2944404>
3. X. H. Su, Z. Liu, G. Y. Lai, Y. Zhang, C. L. P. Chen, Event-triggered adaptive fuzzy control for uncertain strict-feedback nonlinear systems with guaranteed transient performance, *IEEE Trans. Fuzzy Syst.*, **27** (2019), 2327–2337. <https://doi.org/10.1109/TFUZZ.2019.2898156>
4. Y. Liu, X. P. Liu, Y. W. Jing, Adaptive neural networks finite-time tracking control for non-strict feedback systems via prescribed performance, *Inform. Sci.*, **468** (2018), 29–46. <https://doi.org/10.1016/j.ins.2018.08.029>
5. X. W. Yang, W. X. Deng, J. Y. Yao, Disturbance-observer-based adaptive command filtered control for uncertain nonlinear systems, *ISA Trans.*, **130** (2022), 490–499. <https://doi.org/10.1016/j.isatra.2022.04.007>
6. J. Zhang, J. W. Xia, W. Sun, Z. Wang, H. Shen, Command filter-based finite-time adaptive fuzzy control for nonlinear systems with uncertain disturbance, *J. Franklin Inst.*, **356** (2019), 11270–11284. <https://doi.org/10.1016/j.jfranklin.2019.05.042>
7. K. K. Sun, J. B. Qiu, H. R. Karimi, Y. L. Fu, Event-triggered robust fuzzy adaptive finite-time control of nonlinear systems with prescribed performance, *IEEE Trans. Fuzzy Syst.*, **29** (2021), 1460–1471. <https://doi.org/10.1109/TFUZZ.2020.2979129>
8. M. Kharrat, M. Krichen, L. Alkhalifa, K. Gasmi, Neural networks-based adaptive command filter control for nonlinear systems with unknown backlash-like hysteresis and its application to single link robot manipulator, *AIMS Math.*, **9** (2024), 959–973. <https://doi.org/10.3934/math.2024048>
9. B. Guo, S. Y. Dian, T. Zhao, Robust NN-based decentralized optimal tracking control for interconnected nonlinear systems via adaptive dynamic programming, *Nonlinear Dyn.*, **110** (2022), 3429–3446. <https://doi.org/10.1007/s11071-022-07771-2>
10. W. Sun, S. F. Su, Y. Q. Wu, J. W. Xia, Novel adaptive fuzzy control for output constrained stochastic nonstrict feedback nonlinear systems, *IEEE Trans. Fuzzy Syst.*, **29** (2021), 1188–1197. <https://doi.org/10.1109/TFUZZ.2020.2969909>

11. K. K. Sun, L. Liu, J. B. Qiu, G. Feng, Fuzzy adaptive finite-time fault-tolerant control for strict-feedback nonlinear systems, *IEEE Trans. Fuzzy Syst.*, **29** (2021), 786–796. <https://doi.org/10.1109/TFUZZ.2020.2965890>
12. D. Cui, Z. R. Xiang, Nonsingular fixed-time fault-tolerant fuzzy control for switched uncertain nonlinear systems, *IEEE Trans. Fuzzy Syst.*, **31** (2023), 174–183. <https://doi.org/10.1109/TFUZZ.2022.3184048>
13. D. Cui, W. C. Zou, J. Guo, Z. R. Xiang, Adaptive fault-tolerant decentralized tracking control of switched stochastic uncertain nonlinear systems with time-varying delay, *Int. J. Adapt. Control Signal Process.*, **36** (2022), 2971–2987. <https://doi.org/10.1002/acs.3491>
14. H. Q. Wang, P. X. Liu, X. D. Zhao, X. P. Liu, Adaptive fuzzy finite-time control of nonlinear systems with actuator faults, *IEEE Trans. Cybern.*, **50** (2020), 1786–1797. <https://doi.org/10.1109/TCYB.2019.2902868>
15. P. Li, G. H. Yang, Backstepping adaptive fuzzy control of uncertain nonlinear systems against actuator faults, *J. Control Theory Appl.*, **7** (2009), 248–256. <https://doi.org/10.1007/s11768-009-8074-6>
16. Y. Q. Wang, N. Xu, Y. J. Liu, X. D. Zhao, Adaptive fault-tolerant control for switched nonlinear systems based on command filter technique, *Appl. Math. Comput.*, **392** (2021), 125725. <https://doi.org/10.1016/j.amc.2020.125725>
17. M. Chen, G. Tao, Adaptive fault-tolerant control of uncertain nonlinear large-scale systems with unknown dead zone, *IEEE Trans. Cybern.*, **46** (2016), 1851–1862. <https://doi.org/10.1109/TCYB.2015.2456028>
18. L. B. Wu, G. H. Yang, Adaptive fault-tolerant control of a class of nonaffine nonlinear systems with mismatched parameter uncertainties and disturbances, *Nonlinear Dyn.*, **82** (2015), 1281–1291. <https://doi.org/10.1007/s11071-015-2235-6>
19. Z. S. Wang, L. Liu, H. G. Zhang, Neural network-based model-free adaptive fault-tolerant control for discrete-time nonlinear systems with sensor fault, *IEEE Trans. Syst. Man Cybern. Syst.*, **47** (2017), 2351–2362. <https://doi.org/10.1109/TSMC.2017.2672664>
20. Y. Q. Han, Design of decentralized adaptive control approach for large-scale nonlinear systems subjected to input delays under prescribed performance, *Nonlinear Dyn.*, **106** (2021), 565–582. <https://doi.org/10.1007/s11071-021-06843-z>
21. D. Cui, W. C. Zou, J. Guo, Z. R. Xiang, Neural network-based adaptive finite-time tracking control of switched nonlinear systems with time-varying delay, *Appl. Math. Comput.*, **428** (2022), 127216. <https://doi.org/10.1016/j.amc.2022.127216>
22. Z. F. Li, T. S. Li, G. Feng, R. Zhao, Q. H. Shan, Neural network-based adaptive control for pure-feedback stochastic nonlinear systems with time-varying delays and dead-zone input, *IEEE Trans. Syst. Man Cybern. Syst.*, **50** (2020), 5317–5329. <https://doi.org/10.1109/TSMC.2018.2872421>
23. H. Dastres, B. Rezaie, B. Baigzadehnoe, Neural-network-based adaptive backstepping control for a class of unknown nonlinear time-delay systems with unknown input saturation, *Neurocomputing*, **398** (2020), 131–152. <https://doi.org/10.1016/j.neucom.2020.02.070>
24. D. P. Li, Y. J. Liu, S. C. Tong, C. L. P. Chen, D. J. Li, Neural networks-based adaptive control for nonlinear state constrained systems with input delay, *IEEE Trans. Cybern.*, **49** (2019), 1249–1258. <https://doi.org/10.1109/TCYB.2018.2799683>

25. S. Yin, P. Shi, H. Y. Yang, Adaptive fuzzy control of strict-feedback nonlinear time-delay systems with unmodeled dynamics, *IEEE Trans. Cybern.*, **46** (2016), 1926–1938. <https://doi.org/10.1109/TCYB.2015.2457894>
26. T. Wang, J. Wu, Y. J. Wang, M. Ma, Adaptive fuzzy tracking control for a class of strict-feedback nonlinear systems with time-varying input delay and full state constraints, *IEEE Trans. Fuzzy Syst.*, **28** (2020), 3432–3441. <https://doi.org/10.1109/TFUZZ.2019.2952832>
27. B. Niu, L. Li, Adaptive backstepping-based neural tracking control for MIMO nonlinear switched systems subject to input delays, *IEEE Trans. Neural Netw. Learn. Syst.*, **29** (2018), 2638–2644. <https://doi.org/10.1109/TNNLS.2017.2690465>
28. Y. Wu, X. J. Xie, Adaptive fuzzy control for high-order nonlinear time-delay systems with full-state constraints and input saturation, *IEEE Trans. Fuzzy Syst.*, **28** (2020), 1652–1663. <https://doi.org/10.1109/TFUZZ.2019.2920808>
29. H. Q. Wang, S. W. Liu, X. B. Yang, Adaptive neural control for non-strict-feedback nonlinear systems with input delay, *Inform. Sci.*, **514** (2020), 605–616. <https://doi.org/10.1016/j.ins.2019.09.043>
30. Z. J. Yang, X. Y. Zhang, X. J. Zong, G. G. Wang, Adaptive fuzzy control for non-strict feedback nonlinear systems with input delay and full state constraints, *J. Franklin Inst.*, **357** (2020), 6858–6881. <https://doi.org/10.1016/j.jfranklin.2020.05.008>
31. F. Wang, Z. Liu, Y. Zhang, C. L. P. Chen, Adaptive finite-time control of stochastic nonlinear systems with actuator failures, *Fuzzy Sets Syst.*, **374** (2019), 170–183. <https://doi.org/10.1016/j.fss.2018.12.005>
32. Y. Zhang, F. Wang, Adaptive neural control of non-strict feedback system with actuator failures and time-varying delays, *Appl. Math. Comput.*, **362** (2019), 124512. <https://doi.org/10.1016/j.amc.2019.06.026>
33. G. Niedbała, Application of artificial neural networks for multi-criteria yield prediction of winter rapeseed, *Sustainability*, **11** (2019), 1–13. <https://doi.org/10.3390/su11020533>
34. L. Ma, L. Liu, Adaptive neural network control design for uncertain nonstrict feedback nonlinear system with state constraints, *IEEE Trans. Syst. Man Cybern. Syst.*, **51** (2021), 3678–3686. <https://doi.org/10.1109/TSMC.2019.2922393>



AIMS Press

©2024 the Author(s), licensee AIMS Press. This is an open access article distributed under the terms of the Creative Commons Attribution License (<http://creativecommons.org/licenses/by/4.0>)